COO-3158-48

DEFECTS IN METAL CRYSTALS

Progress Report
for Period May 1, 1975 - April 30, 1976

D. N. Seidman

Cornell University
Ithaca, New York 14853

February 1976

Prepared for

THE U.S. ENERGY RESEARCH AND DEVELOPMENT ADMINISTRATION
UNDER CONTRACT NO. E(11-1)-3158

DISCLAIMER

DEFECTS IN METAL CRYSTALS

D. N. Seidman

ABSTRACT

The objective of the present research effort was a broad investigation of the properties of crystal defects in metal crystals. Attention was focused on point defects (vacancies, interstitials and solute atoms), aggregates of point defects and their interactions with one another. A strong emphasis was placed on the use of different irradiating species (300-700eV Xe^+ ions, 20-30keV W^+ ions, 20-30keV Mo^+ ions, and fast neutrons) to introduce both vacancies and interstitials in a number of different pure metals (Mo, W, Au) and alloys [Pt-(Au), W-(Re), Mo(Ti), Ni_4Mo, low-swelling 316 stainless steels and commercial 316 stainless steels].

Progress was made in the following areas:

(A) An <u>In-Situ</u> Field-Ion Microscope Study of Ion-Irradiated Tungsten and Tungsten Alloys.

1. The Recovery Behavior in Stages I and II of Pure Tungsten.
2. The Recovery Behavior in Stages I and II of Tungsten-(Rhenium) Alloys.

(B) The Study of Stages I to IV of Irradiated or Quenched Tungsten and Tungsten Alloys by Field-Ion Microscopy: A Review

(C) Field-Ion Microscope Studies of the Defect Structure of the Primary State of Damage of Irradiated Metals: A Review

(D) An <u>In-Situ</u> Field-Ion Microscope Study of the Recovery Behavior of Ion-Irradiated Molybdenum in Stages I and II.

(E) A Field-Ion Microscope Study of the Recovery Behavior of Stage II in a Series of Ion-Irradiated Platinum-0.10, 0.62 and 4.0 at.% Gold Alloys.

(F) A New Technique for Focused-Collision Sequence Range Measurements

(G) Atom-Probe Field-Ion Microscopy

1. Technical Improvements in the Atom-Probe FIM

   a) Resolution

   b) Low-Energy Ion-Gun

   c) Residual gas analyzer

2. Results

   a) Tungsten and tungsten alloys

   b) Molybdenum and molybdenum alloys

      i) molybdenum

      ii) titanium-zirconium-molybdenum (TZM)

      iii) molybdenum-(titanium)

   c) A low swelling stainless steel alloy (LSIA)

H. The Range of a Focused Collision Replacement Sequence in Ordered Alloys

I. The Interaction of Self-Interstitial Atoms with Impurity Gas Solute Atoms in Refractory Metals

1. INTRODUCTION

During the past year a number of projects was completed, and significant progress was made in other areas. A brief account of the work is given in Section II.

The following personnel were involved:

Professor D.N. Seidman, Principal Investigator

Dr. G. Ayrault, Research Associate (joined October 1973)

Dr. T.M. Hall, Research Associate (joined May 1973)

J. Aidelberg, Research Assistant (joined September 1974)

C. H. Nielsen, Teaching Assistant (left February 1976)

I. Sun, Research Assistant (joined September 1974)

A. Wagner, IBM Fellowship Holder (joined September 1972)

C. Y. Wei, Research Assistant (joined September 1971)

K. Pratt, Film Scanner (joined March 1970)

R. Whitmarsh, Technician (joined January 1968)

II. EXPERIMENTAL WORK

A. An In-Situ Field-Ion Microscope Study of Ion-Irradiated Tungsten and Tungsten Alloys.

1. The Recovery Behavior in Stages I and II of Pure Tungsten

The low-temperature field-ion microscope (FIM) isochronal annealing spectrum of pure tungsten irradiated in-situ with 30keV W^+ ions to a standard dose of $5 \cdot 10^{12}$ ions cm^{-2} at 18K had been shown by Scanlan et al. (1,2) and Wilson and Seidman (3,4,5) to consist of distinct recovery peaks at $\sim$38, 50, 65 and 80K with a small amount of recovery observed up to 120K. They ascribed a process of self-interstitial atom (SIA) long-range migration in Stage I to the 38K peak and calculated an enthalpy change of migration of 0.085eV. However, recent internal friction results published by Okuda and Mizubayashi (6) implied that the process of SIA long-range migration occurrs at $\sim$15K. In addition, a dose and impurity concentration dependent recovery substage in tungsten between 24 and 30K had recently been reported by Dansinger and Schultz (7); hence

they ascribed this substage to uncorrelated long-range migration of an SIA. To investigate the possibility of the existence of SIA long-range migration below 30K the experiments of Scanlan et al. and Wilson and Seidman were carefully repeated. The experimental procedure was modified to allow for a lower irradiation temperature (T_o = 6K) and a slower heating rate <2K min^{-1} .

The results of the FIM isochronal annealing experiments indicate that there is no appreciable recovery below 20K. This observation is not consistent with the internal friction results of Okuda and Mizubayashi (6). However, an analysis of the isochronal annealing experiments revealed that the observed recovery between 20 and 40K is too broad to represent a single thermally-activated diffusion process. This conclusion was reached by superimposing an analytical recovery curve, based on a diffusion treatment of the FIM situation (2), on the FIM isochronal recovery peak centered at 38K. Further details are available in the M.S. thesis of C.H. Nielsen (8).

2. The Recovery Behavior in Stages I and II of Tungsten-(Rhenium) Alloys.

Direct evidence for the formation of SIA-rhenium atom complexes in 30keV W^+ ion-irradiated tungsten-(rhenium) alloys in Stage I had been reported by Wilson and Seidman (4). They observed a radical suppression of the 38K substage of the FIM isochronal annealing spectrum as a result of the addition of rhenium to tungsten. In order to determine the kinetics of the detrapping mechanism a search for the release temperature was carried out using the isochronal FIM annealing technique. Tungsten specimens, alloyed with 1 and 3 atomic % rhenium were irradiated in-situ with 30keV W^+ ions at 15K to a standard dose of $5 \cdot 10^{12}$ ions cm^{-2} and were subsequently annealed to $\sim$400K at a rate of $\sim$2.5K min^{-1}. The FIM isochronal recovery spectra were observed to contain no unambiguous release peaks analogous to those reported by Wei and Seidman for Pt-.0.62%Au alloys (9). This result indicated that the SIA-rhenium atom complex had a binding enthalpy of at least 0.8eV assuming that the dissociation enthalpy could be taken as the sum of the binding

enthalpy and the motion enthalpy of the SIA (10).

Post-anneal pulse-field evaporation experiments revealed several isolated complex-contrast patterns randomly distributed throughout the sampled volume of the specimen. A total of $1.1 \cdot 10^5$ atoms were counted and 11 complex patterns observed, thus implying a concentration of $\sim 1 \times 10^{-4}$ at.fr. The complex pattern consisted of vacant sites on two to three successive layers and was usually terminated by one or two extra bright spots. These patterns were different from any of our earlier strain-field contrast effects; they were also different from both the Stage I SIA and the rhenium atom contrast patterns. However, the patterns were somewhat similar to those observed by Wilson and Seidman (11) in 2.35 MeV electron-irradiated tungsten; Wilson and Seidman (11) irradiated their specimens just below stage III ($\simeq$430K) to a close-pair concentration (before recombination) of $\sim 4 \times 10^{-3}$ at.fr. and examined them at 18K; it was found that the tungsten specimens contained a complex pattern concentration of 1×10^{-4} at.fr. These researchers suggested that the unusual patterns resulted from either SIA clusters or SIA-impurity atom clusters.

It was therefore concluded that the tungsten SIA's remained trapped up to $\sim$400K and that the complex contrast patterns represented a direct observation of the tungsten SIA-rhenium atom clusters.

B. The Study of Stages I to IV of Irradiated or Quenched Tungsten and Tungsten Alloys by Field-Ion Microscopy: A Review

An invited review article (12) was prepared for the International Conference on "Fundamental Aspects of Radiation Damage in Metals" held in Gatlinburg, Tennessee during October 5-19, 1975. In this article the progress made at Cornell since 1972 in applying the quantitative field-ion microscope (FIM) technique to the study of point defects in irradiated tungsten and tungsten alloys or quenched tungsten is reviewed. The emphasis had been placed on ascertaining recovery mechanisms for the major recovery stages which are consistent with both other FIM observations as well as observations employing more macroscopic techniques; hence point defect

recovery models were presented for recovery Stages I to III. The following conclusions were reached: (1) the value of the volume change of migration (Δv_{1i}^{m}) for the Stage I SIA is less than $0.02\Omega_a$; (2) a strong SIA long-range migration peak was found at ∿38K; (3) Stage I must terminate at ≲45K and not 100K as had been suggested by earlier researchers; (4) the maximum possible downward T shift of the 38K peak was <10K due to the $p\Delta v_{1i}^{m}$ effect; (5) the isochronal recovery spectra of 4 different purity levels (R=15 to 5×10^{4}) of 30keV W^{+} ion-irradiated W were essentially identical between 18 and 120K; (6) these 4 different purity level W specimens exhibited a distinct series of long-range migration recovery peaks at ∿38, 50, 65 and 80K with a small amount of recovery observed up to 120K; (7) conclusions (5) and (6) indicate that the distribution of SIA's produced by the 30keV W^{+} ion irradiations was such that the SIA's only interacted weakly with the impurity atoms and that the SIA-SIA reaction dominated the recovery behavior; (8) the long-range migration peaks fit a diffusion-limited annealing model; (9) the FIM experiments provided direct evidence for the long-range migration of both SIA's and SIA clusters in Stage II between ∿45 and 120K; (10) the FIM observations of SIA long-range migration in Stages I and II are in agreement with the Dausinger-Schultz (7) results if a T shift of ∿5 to 6.5K is made to superimpose the long-range migration peaks in the two sets of data; (11) the binding enthalpy of an SIA to a C atom is ∿0.03eV and the binding enthalpy of an SIA to a Re atom is >0.8eV; (12) no evidence has been found for isolated thermally converted SIA's (the Stage III SIA) at a concentration above 5×10^{-6} at.fr. at $T_i \simeq 430$K for W electron irradiated to a dose of $\sim1\times10^{20}$ cm^{-2}; (13) it was argued that in the Attardo et al. (13) experiments that the transmutation of W to Re, as a result of a thermal neutron dose of $\sim10^{20}$ cm^{-2}, caused a large number of SIA's to become trapped at Re atoms and that the contrast effect they observed after a 60°C irradiation was due to a Re-SIA complex; and (14) the W quenching experiments of Kunz and Shcultz (14), Gripshover et al. (15) in conjunc-

tion with the prequenching and electron irradiation experiments of Kunz et al. (16) and the combined FIM-resistivity study of Park et al. (17) indicate that the quenched-in resistivity increment may consist of mainly dispersed impurity-atoms, vacancy-impurity atom clusters and a small concentration of monovacancies.

C. Field-Ion Microscope Studies of the Defect Structure of the Primary State of Damage of Irradiated Metals: A Review

An invited review article (18) was prepared for the "Materials Science Seminar: Radiation Damage in Metals" held at the Materials Science Symposium in Cincinnati, Ohio during November 9 and 10, 1975. This paper reviewed the application of the FIM technique to the problem of determining directly the spatial distribution of point defects produced by an energetic primary knock-on atom (PKA). Attention was focused specifically on the primary state of damage (i.e., the point-defect distribution without a post-irradiation anneal) produced by energetic heavy-ions (e.g., 20-100keV W^+, Xe^+ or Ar^+) and fast neutrons (energy > 1MeV) in the metals tungsten, iridium and platinum; the simpler primary state of damage produced by MeV electrons was not considered. A review was first given of the theoretical concept of a depleted zone and the role played by both focusons and focused replacement collision sequences in its development. A brief discussion of the physical concepts (field ionization, field evaporation, and resolution) involved in understanding the FIM technique was also presented. It was emphasized that the FIM technique is the only one presently capable of determining the spatial distribution of point defects within and around a depleted zone.

The Cornell FIM research on depleted zones was reviewed in detail. The emphasis in this work was on determining the point-defect structure of a depleted zone produced by a single ion. The irradiating ion used was the self-ion (W^+) to avoid any possible problems associated with the introduction of impurity atoms in the lattice as a result of the irradiation. Each depleted zone was created in an almost initially perfect crystal lattice (i.e., the tip volume of $\sim 10^{-16} cm^3$). Two

different irradiation temperatures (T_i) were employed; 473 and 18K. The T_i of 473K is towards the top of Stage II and is therefore above the temperature of long-range migration of the Stage I SIA, but below the temperature where monovacancies migrate. The T_i of 18K is below the onset of long-range migration of SIA's in Stage I. A detailed discussion of the results of these experiments can be found in reference 18 plus our earlier publications (19,20).

The work of other groups on the primary state of radiation damage in the metals tungsten, iridium and platinum was also reviewed. The emphasis of most of this work had been on characterizing the distribution of vacancy damage produced at room temperature, and in a few experiments, at 78K. Typically only large clusters of vacancies (i.e., greater than 10 vacancies) had been studied as the minimum field evaporation increment, for a high index plane, was one atomic layer. This coarse an increment precludes almost a priori obtaining detailed information about the point-defect structure of a depleted zone. Nevertheless, this research has been useful in demonstrating that basically three morphological types of vacancy damage exists in the primary state of damage. These three basic types are: (1) depleted zones; (2) compact vacancy clusters or voids; and (3) dislocation loops. The voids may be considered to be depleted zones with a very high vacancy concentration, since the experimental work was not able to prove that the voids only consisted of vacancies. The dislocation loops are depleted zones that have collapsed into the lower-energy dislocation loops.

The important result that emerges from the FIM research on both tungsten and iridium is that the dislocation loop portion of the damage accounts for only a small fraction of the total vacancy population. The remaining fraction of the vacancy population (90% in the case of tungsten) is in the form of depleted zones (with a vacancy concentration of between 1 and 20at.%) and compact clusters (voids). These observations offer an explanation of why the yield factor (Y), where

$$Y = \frac{\text{observable vacancy loops (number per cm}^2\text{)}}{\text{ion dose (number of ions per cm}^2\text{)}},$$

measured by TEM is often considerably less than unity. For example, in the case of copper irradiated with 30keV Cu^+ ions at room temperature Y is 0.3 (21), and in the case of tungsten irradiated at room temperature it is 0.1 (52,73). This is an extremely important point because the TEM technique has been extensively used to study vacancy damage in both self-ion and neutron irradiated metals (22,23,24). The observation of the primary radiation damage state by TEM depends heavily on the ability of the vacancy-rich core of a depleted zone to collapse into a dislocation loop with sufficient strain-field contrast to make itself "visible" in an electron microscope image. Thus the FIM observations provide a simple explanation of the low yield-factor, determined by transmission electron microscopy, for a number of ion-irradiated metals.

D. An In-Situ Field-Ion Microscope Study of the Recovery Behavior of Ion-Irradiated Molybdenum in Stages I and II.

The mobility of single molybdenum SIA's was studied in a series of in-situ FIM experiments. High purity (resistivity ratio of ∿5700) molybdenum specimens were irradiated with 30keV Mo^+ ions to a standard dose of $5 \cdot 10^{12}$ ions cm^{-2} at 10K. Subsequent isochronal annealing experiments were performed at a heating rate of ∿2.5K min^{-1} between 10 and 120K. The low temperature annealing spectrum was shown to consist of distinct recovery peaks at 32, 45 and 70K as seen in Fig. 1. The major peak at 32K was considered to represent the onset of long-range migration and was found to closely obey the analytical shape predicted by a diffusion model (2).

The effect of the imaging electric field on the mobility of the SIA was studied in a series of control experiments. The experimental procedure involved irradiating molybdenum specimens in-situ at 40K in the absence of any electric field, and then cooling to 15K. Isochronal annealing experiments were then performed in the presence of the field. The results of these experiments demonstrated that

Figure 1. A composite FIM isochronal spectrum of 4 spectra for molybdenum irradiated at 10K with 30keV Mo^{+} ions to a dose of $5x10^{12}$ ion cm^{-2} and warmed to 120K at a rate of $\sim$2.5K min^{-1}.

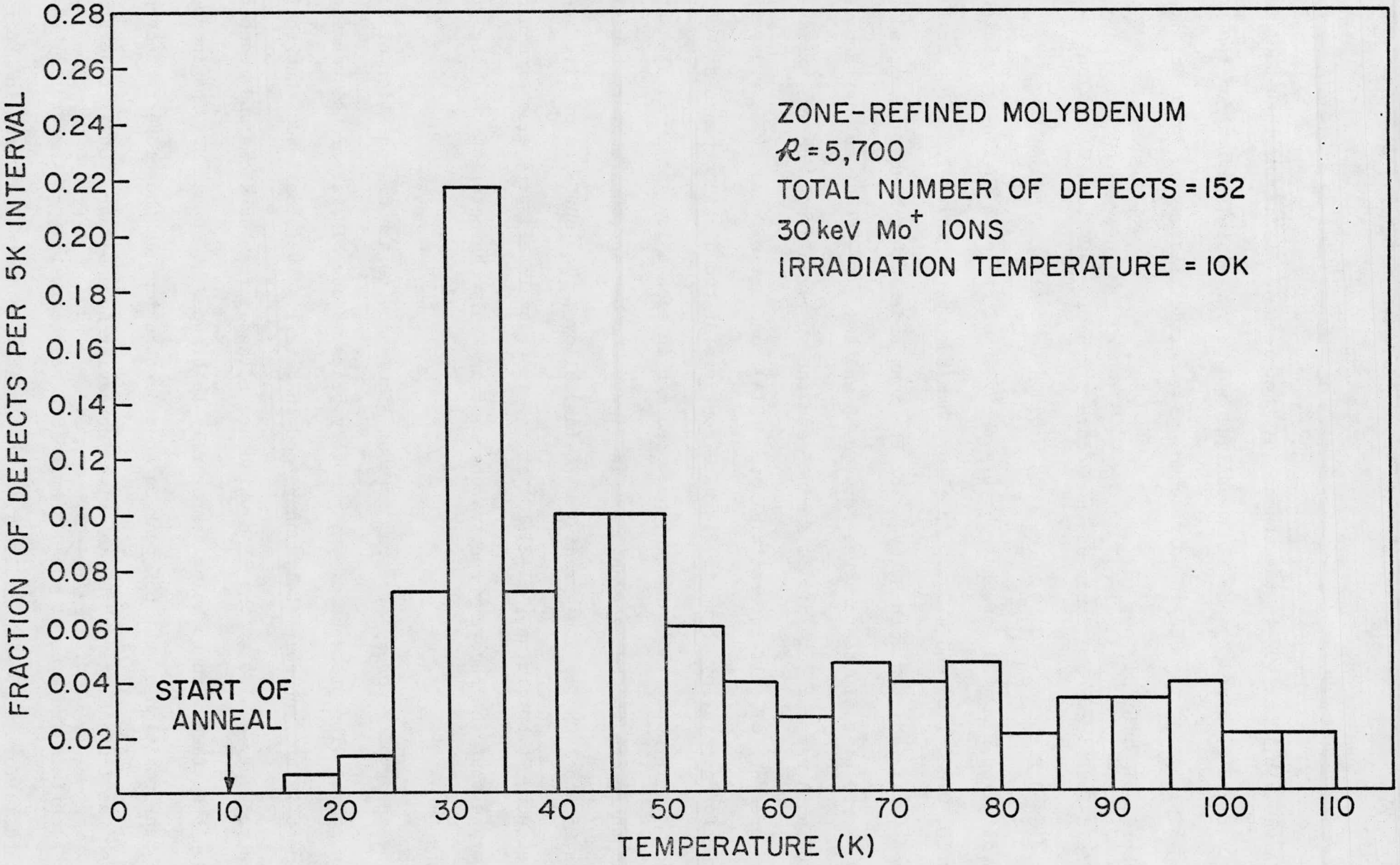
ZONE-REFINED MOLYBDENUM
R = 5,700
TOTAL NUMBER OF DEFECTS = 152
30 keV Mo+ IONS
IRRADIATION TEMPERATURE = 10K
FRACTION OF DEFECTS PER 5K INTERVAL
0.28
0.26
0.24
0.22
0.20
0.18
0.16
0.14
0.12
0.10
0.08
0.06
0.04
0.02
START OF ANNEAL
0
10
20
30
40
50
60
70
80
90
100
110
TEMPERATURE (K)

Figure 1

the SIA was mobile at 40K in the absence of the electric field, and that the large electric field required by the FIM technique had only a minimal effect on the annealing kinetics of the SIA in molybdenum. Further details may be found in the M.S. thesis of C. H. Nielsen (8).

E. A Field-Ion Microscope Study of the Recovery Behavior of Stage II in Ion-Irradiated Platinum - 0.10, 0.62, and 4.0at.% Gold Alloys

A detailed FIM study of the recovery behavior of Stage II in ion-irradiated Pt - 0.10, 0.62, (10) and 4.0at.% Au alloys has been performed. Typically an FIM specimen was irradiated with 30keV W^+ or Pt^+ ions under ultra-high vacuum conditions ($\leq 2.10^{-9}$Torr) at a tip temperature between 35 and 40K. The specimen was then warmed to $\geq$100K at a warming rate of $\sim$1.5K min^{-1} and the specimen's surface was examined for the presence of self-interstitial atom (SIA) contrast effects. The recovery spectrum for each alloy shown in figure 2 consists of two distinct peaks at $\sim$68 and 88K. It is noted that at least one specimen in each alloy was irradiated at 25K and therefore the recovery spectra in figure 2 represent the recovery behavior between 25 and 100K for ion-irradiated Pt-(Au) alloys. The surfaces of five irradiated pure Pt specimens [$\sim(1\text{-}2)\cdot 10^{-5}$at.fr. impurity level] were also examined to demonstrate that the recovery spectra observed are only characteristic of the Pt-(Au) alloys.

The observed recovery spectrum is most likely due to the dissociation of SIAs from Au atoms. The presence of two recovery peaks in our FIM isochronal warming experiment is not yet completely understood in detail. It is believed that the 68K peak is probably caused by the SIAs which are released from Au atoms and reach the specimen's surface without being temporarily re-trapped at Au atoms. The independence of the peak position of the 68K peak on Au concentration can therefore be understood and also the increasing peak height with increasing Au concentration is understandable. A certain fraction of the detrapped SIA may be re-trapped temporarily at Au atoms and perform a hopping motion from one Au atom to another Au atom in their

Figure 2. The composite spectra for the isochronal recovery of Pt-0.10, 0.62, and 4.0at.% Au alloys which were irradiated mainly between 35 and 40K with 30keV W^+ or Pt^+ ions and then warmed at a linear rate of $\sim$1.5K min^{-1} to 100K.

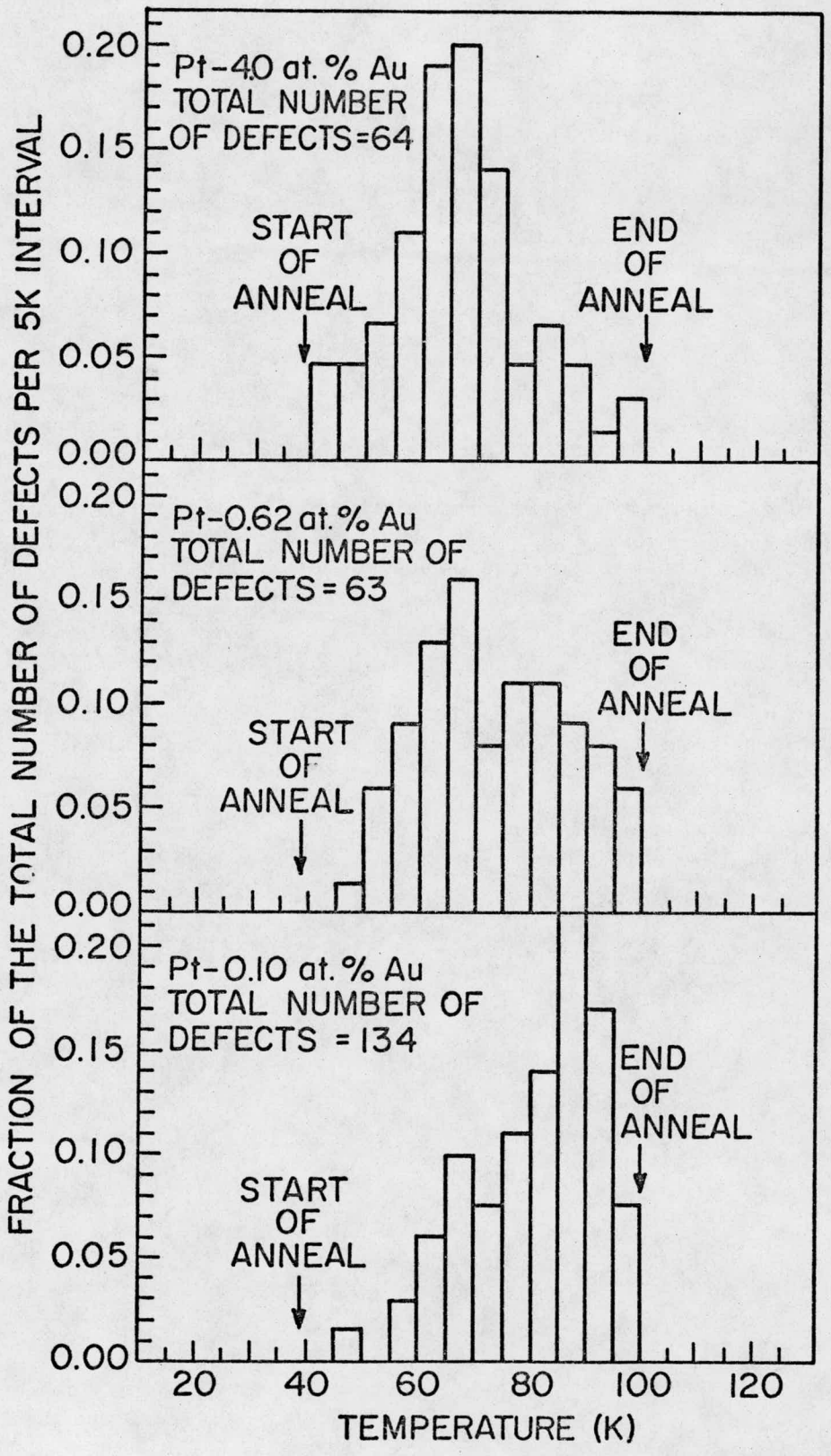
Pt-4.0 at. % Au
TOTAL NUMBER
OF DEFECTS=64
START
OF
ANNEAL
END
OF
ANNEAL
Pt-0.62 at. % Au
TOTAL NUMBER OF
DEFECTS = 63
START
OF
ANNEAL
END
OF
ANNEAL
Pt-0.10 at. % Au
TOTAL NUMBER OF
DEFECTS = 134
START
OF
ANNEAL
END
OF
ANNEAL
FRACTION OF THE TOTAL NUMBER OF DEFECTS PER 5K INTERVAL
0.00
0.05
0.10
0.15
0.20
20
40
60
80
100
120
TEMPERATURE (K)

Figure 2

journey to the specimen's surface. These SIAs then constitute the recovery peak at 88K. Questions concerning the peak position and the peak height for the 88K peak cannot be answered at the present time. If SIAs in 88K peak perform a hopping motion from one Au atom to another Au atom, we would expect according to an impurity-delayed diffusion model that the position of the peak should shift to higher temperatures as the Au concentration is increased. Obviously, the 88K peak observed does not behave exactly as is expected. Two possible mechanisms are considered: (1) the trapping of SIA's at deeper traps such as di-Au atoms or (2) the smaller separation between SIAs and depleted zones in the higher concentration gold alloys. In mechanism (1) it is expected that in the higher concentration gold alloys more SIAs are trapped at di-Au atoms and therefore survive recovery in the 88K peak. On the contrary, in mechanism (2) fewer SIAs trapped at di-Au atoms may be expected since more SIAs probably return to the depleted zones where they originated. In order to reach a better judgment a series of post-annealing peeling experiments for each alloy are being studied. An FIM specimen was first ion-irradiated between 35 and 40K to a dose of $\sim 1 \cdot 10^{13}$ ion cm^{-2}, then warmed to ~100K in the presence of the imaging electric field and finally peeled at 70K to search for the concentration of SIAs remaining the anneal to 100K. The film from these experiments are currently being analyzed and the final results will be reported during the coming year.

F. A New Technique for Focused Collision Sequence Range Measurements.

One of the most persistent problems in the field of radiation damage is that of understanding the nature of the initial damage event; i.e., the spatial distribution of vacancies and self-interstitial atoms produced as the result of the impact of an energetic particle. Since Silsbee (25) first introduced the concept of focused collision sequences (FCS) in 1957, these events have often been discussed as a determining factor in the initial spatial distribution of damage. However, due to experimental difficulties, the range of these events, and even proof of their

existence, has remained somewhat elusive. Indeed in gold, FCS ranges of <50Å (26) and 4000Å or more (27) have been proposed. Clearly, further work is needed to rationalize this immense disparity, and in a more general sence to understand the role of focusing in radiation damage. Toward this end we have developed a unique, and direct technique for studying focused collision sequences.

The present series of experiments is being carried out on gold, although the technique should be applicable to other metals as well. The specimens are epitaxially grown, vapor deposited single crystals which range from 400 to 1500Å in thickness. Experiments to date have been carried out on crystals with <100> film normals, but films of other orientations (<110> and <111>) are now being prepared in order to study crystallographic effects. The films are bombarded with low energy ($\lesssim$700eV) Xe^+ ions directed along the film normal, using the ion gun and specimen holder shown in Fig. 3. Focused collision sequences with a range greater than the film thickness can cause the ejection of atoms as ions from the bottom surface of the film. These ions are detected using the Bendix Channeltron Electron Multiplier Array (CEMA) system shown in Fig. 3, which consists of two individual CEMAs placed in series. The output from this is detected both visually (with a fluorescent screen) and electronically. The experiments are carried out in the high vacuum system ($\sim 5 \times 10^{-8}$ torr) shown in Fig. 4. As indicated, the specimen holder is mounted on the tail section of a continuous transfer liquid helium cryostat, with which the specimen can be maintained at any temperature between 25 and 300K. In order to ensure that the observed current emerging from the bottom surface of the film is not due to channeling of light in impurities (H^+ or He^+), the magnetic separator shown in Fig. 3 is placed in the beam path. This magnetic analyzer removes any light ion component from the beam.

Early experiments (28) on this system were carried out using visual detection of the CEMA output, with a fluorescent screen. Visual observation was adequate to demonstrate the existence of a long FCS range in gold (>800Å). After this observa-

Figure 3. Experimental apparatus for the study of focused collision sequences showing the ion gun, the magnetic beam analyzer, the specimen holder, and CEMA detector.

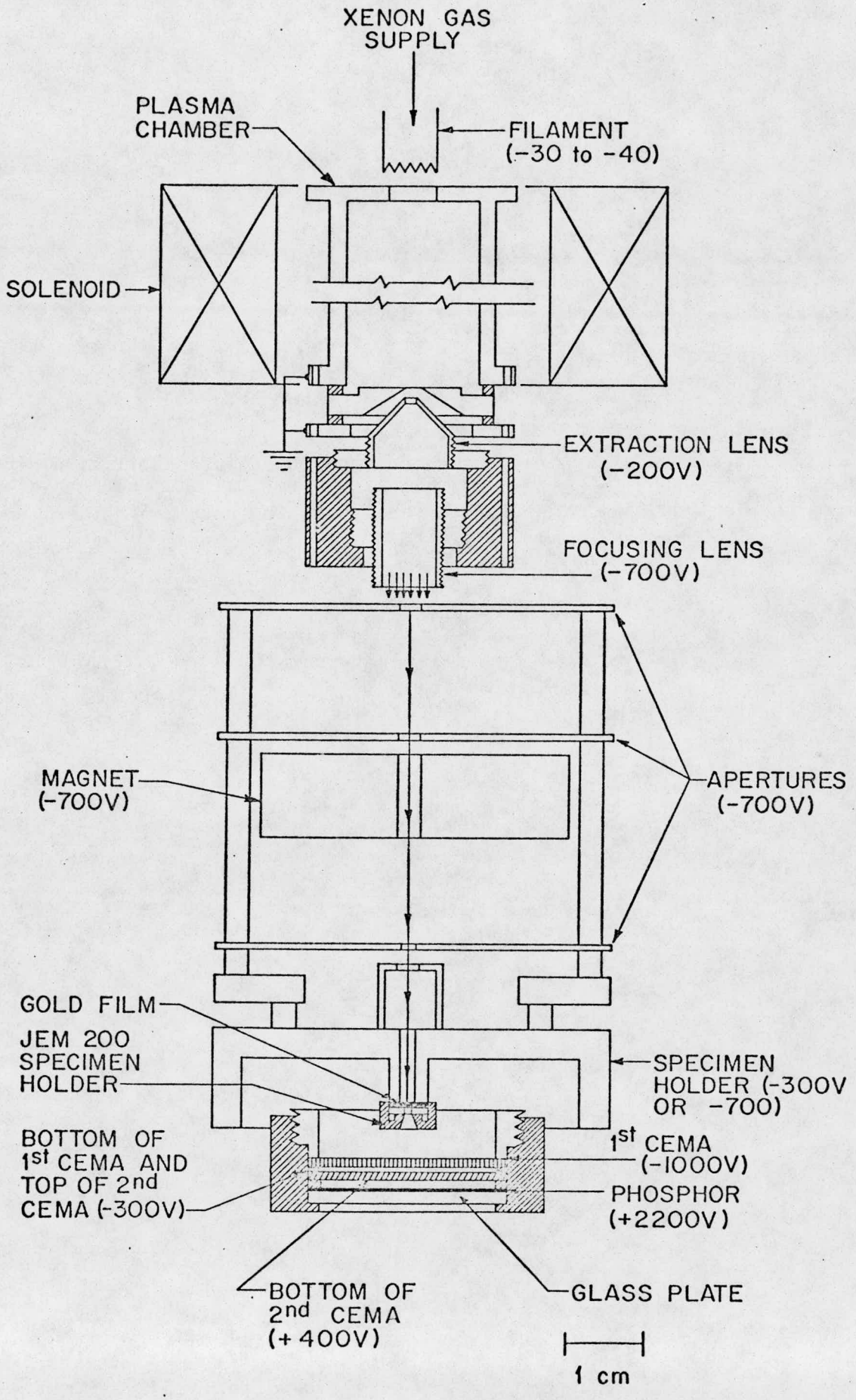
XENON GAS SUPPLY
PLASMA CHAMBER
FILAMENT (-30 to -40)
SOLENOID
EXTRACTION LENS (-200V)
FOCUSING LENS (-700V)
MAGNET (-700V)
APERTURES (-700V)
GOLD FILM
JEM 200 SPECIMEN HOLDER
SPECIMEN HOLDER (-300V OR -700)
BOTTOM OF 1st CEMA AND TOP OF 2nd CEMA (-300V)
1st CEMA (-1000V)
PHOSPHOR (+2200V)
BOTTOM OF 2nd CEMA (+400V)
GLASS PLATE
1 cm

Figure 3

Figure 4. Experimental system: (A) electrostatic lens: (B) sapphire strip; (C) platinum resistance thermometer; (D) machinable glass ceramic detector mount; (E) Channeltron Electron Multiplier Arrays; (F) fluorescent screen; (G) specimen holder; (H) beam apertures; (I) liquid helium cryostat; (J) copper block; (K) copper specimen mounting block; (L) magnet; (M) insulator.

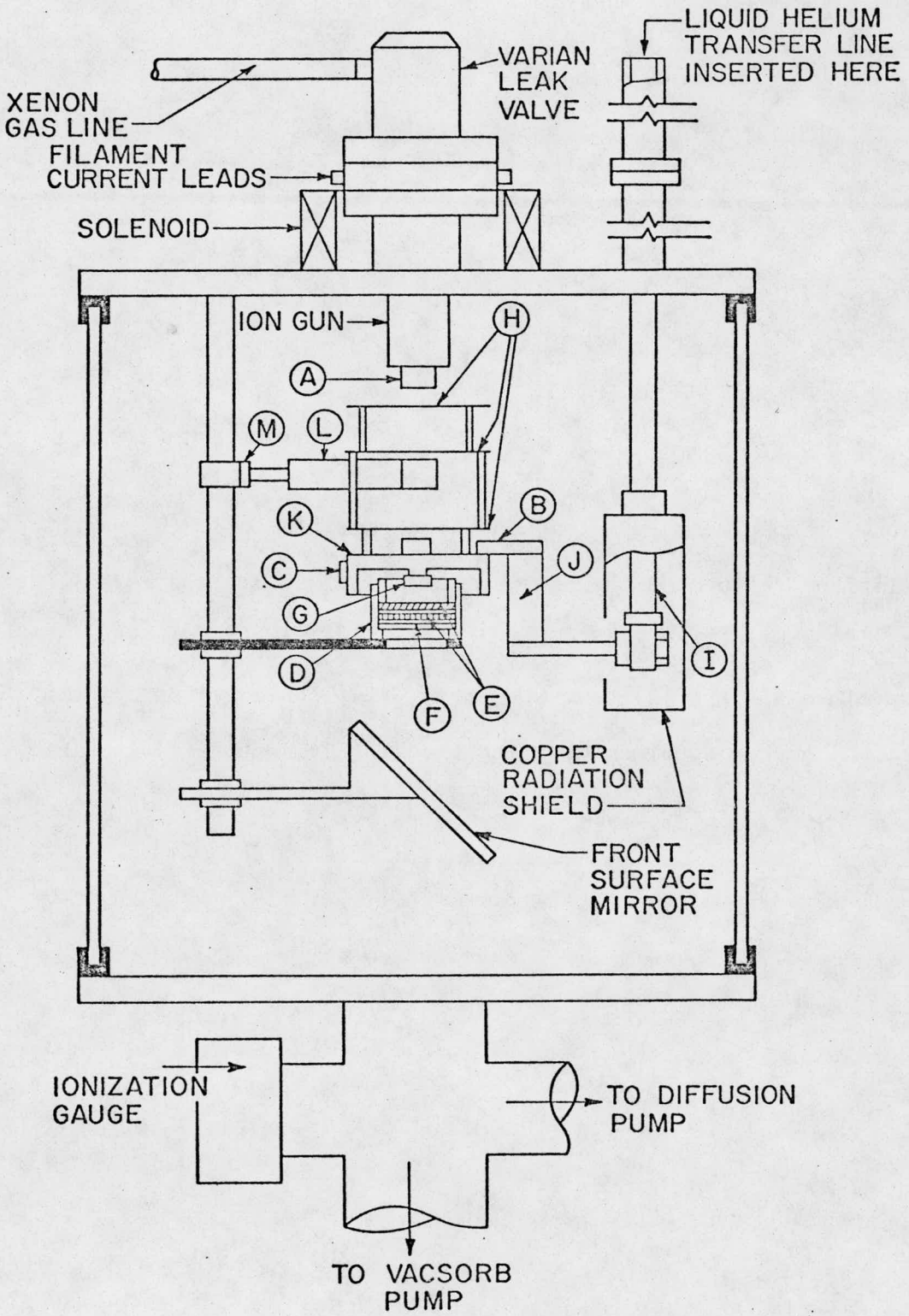
LIQUID HELIUM
TRANSFER LINE
INSERTED HERE
VARIAN
LEAK
VALVE
XENON
GAS LINE
FILAMENT
CURRENT LEADS
SOLENOID
ION GUN
H
A
M
L
B
K
C
J
G
I
D
F
E
COPPER
RADIATION
SHIELD
FRONT
SURFACE
MIRROR
IONIZATION
GAUGE
TO DIFFUSION
PUMP
TO VACSORB
PUMP

Figure 4

tion it was decided that a sensitive quantitative system was needed to measure the small signals from thicker films, and the large outputs from thinner films. This system would give us the capability of quantitatively measuring the output versus thickness in films free of radiation damage, and also measuring the effect of radiation damage on the FCS range.

For these reasons, the electronic measuring system shown in Fig. 5 has been built, and is now in regular operation. The Xe^+ ion beam is pulsed at a known frequency ($\sim$100 Hz) by pulsing the ion-gun filament bias. Each pulse produces a burst of separate events in the CEMA; every burst is caused by a simple ion emerging from the bottom surface of the film. These events are individually amplified and then averaged (with a time constant which is short compared to the 100Hz beam pulsing frequency) and fed into an Ithaco model 391A lock-in amplifier (LIA), operating at the 100Hz ion pulse frequency. This synchronous detection system gives a very precise measure of the detector output, with a high degree of noise rejection.

Since the output is proportional to the input ion current, the variable of interest is the ratio of the output to this current. This is provided directly by a current measuring circuit linked to a ratiometer built into the LIA. Both this ratio and the direct LIA output are recorded on a dual pen strip chart recorder.

The newly installed electronic measuring system has yielded surprising results. On undamaged films, the dependence of output current on foil thickness is as expected; thin foils yield larger output currents than thick foils. However, as the foil is irradiated (and therefore damaged) and sputter-thinned by the Xe^+ ion beam, the output current does not rise as expected, but instead decreases. This behavior may be due to a defocusing effect caused by the radiation damage. This effect, along with the temperature and ion energy dependence of the FCS range in gold are presently being studied. The dependence on crystallographic orientation is scheduled for study in the very near future.

Figure 5. A schematic diagram of the electronic system used to measure the ion-current ejected from the bottom surface of the thin film.

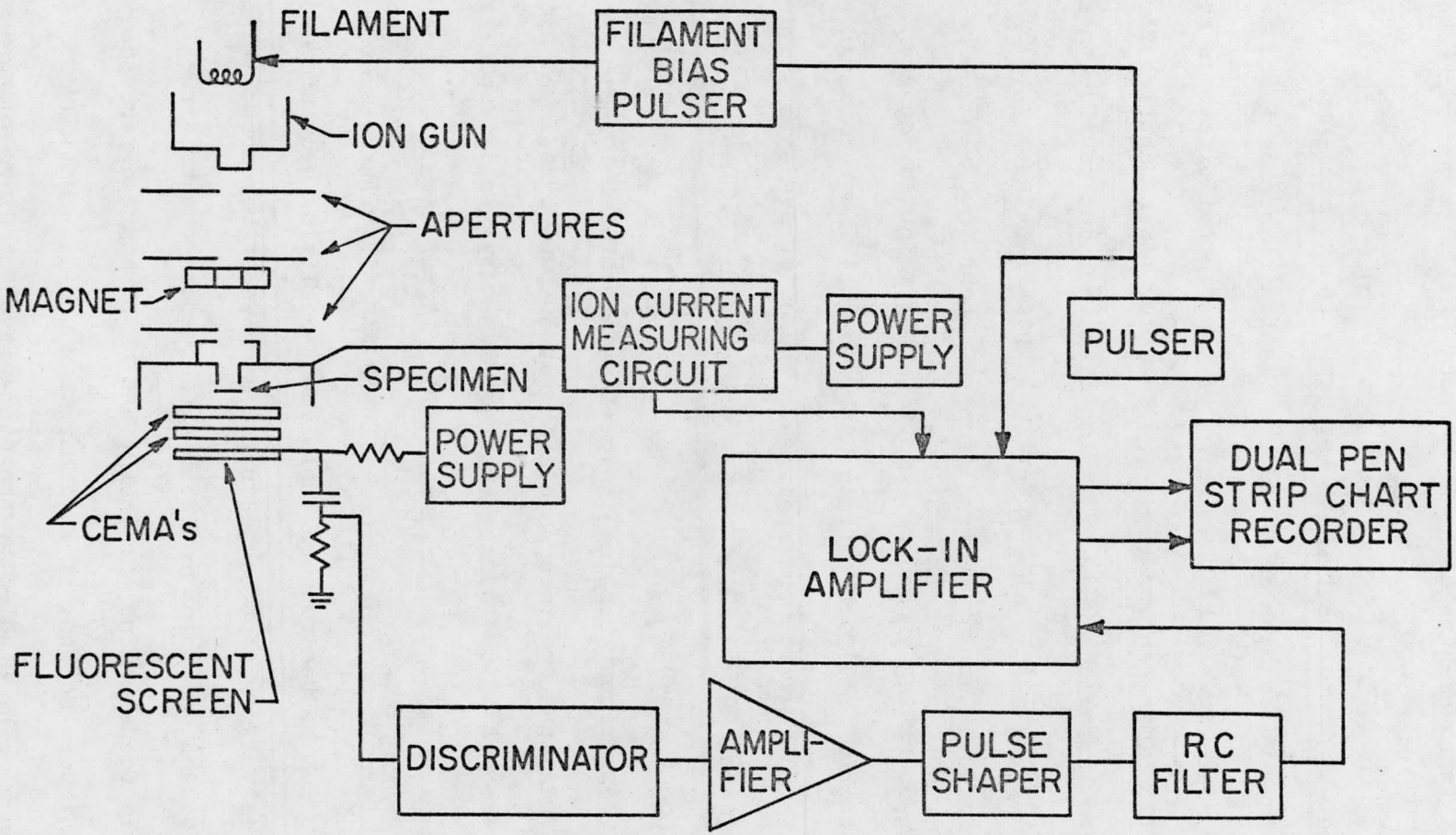
FILAMENT
FILAMENT BIAS PULSER
ION GUN
APERTURES
MAGNET
ION CURRENT MEASURING CIRCUIT
POWER SUPPLY
PULSER
SPECIMEN
POWER SUPPLY
DUAL PEN STRIP CHART RECORDER
LOCK-IN AMPLIFIER
CEMA's
FLUORESCENT SCREEN
DISCRIMINATOR
AMPLI-FIER
PULSE SHAPER
R C FILTER

Figure 5

G. Atom-Probe Field-Ion Microscopy

1. Technical Improvements in the Atom-Probe FIM

(a) Resolution

Several technical improvements have been made in the atom-probe FIM and in the operational technique which have improved the resolution of the instrument. The improvements were as follows: (1) The design of the digital timer was modified to eliminate systematic timing errors (29); (2) Tracking power supplies for the dc and pulse voltages were installed (29). This improves the mass resolution and simplifies the mass calibration of the time-of-flight spectrometer; and (3) The regularly obtainable background vacuum was reduced from $\lesssim 10^{-8}$ torr to $\lesssim 5 \times 10^{-10}$ torr by a number of improvements in operating procedure. This latter point is important because it reduces the number of artifact effects caused by the interaction of residual impurity gases interacting with the specimen. These improvements are described in detail in references 29 and 30.

(b) Low-Energy Ion-Gun

A preliminary experiment testing the performance of the low-energy gas ion-gun was conducted. A tungsten specimen maintained at 30K was irradiated with 275eV Ne^+ ions. After the removal of the damaged surface layer by field-evaporation an isochronal annealing experiment was performed. This latter experiment revealed the presence of SIAs migrating to the surface of the FIM tip. These SIAs were most likely produced at 30K by the focused replacement collision sequence mechanism.

This preliminary experiment suggests two avenues of research. First, range measurements of focused collision replacement sequences can be directly measured. It is also possible to determine the energy and temperature depencence of the range by this same technique. Second, it is clear that the interaction of SIAs with impurity atoms can also be studied by the atom-probe technique where the SIAs are introduced by low-energy bombardments.

(c) Residual Gas Analyzer

A Uthe Technology Inc. (UTI) Model 100C residual gas analyzer was installed on the atom-probe FIM. The analyzer allows us to determine the composition of the residual gases in the vacuum system. This instrument has proved to be particularly valuable for determining whether specific impurity atoms originated in the specimen or were artifacts of the vacuum conditions. This instrument has also proven particularly valuable for determining the CO and CO_2 levels in the vacuum system, thus aiding in the interpretation of the peaks observed at atomic mass 16 which could be due either to titanium in a specimen or oxygen from the vacuum system.

2. Results

A number of both pure metals and alloys have been examined in the atom-probe FIM including tungsten, tungsten-rhenium, molybdenum, molybdenum-titanium, TZM (titanium-zirconium-molybdenum) alloy, and a low swelling stainless steel (LSIA).

(a) Tungsten and Tungsten Alloys

Tungsten and tungsten alloys were investigated to develop an operational technique that would be suitable for experiments on the neutron irradiated samples of tungsten and tungsten-rhenium that have been supplied by Dr. F. W. Wiffen of the Oak Ridge National Laboratory.

Figure 6 shows data recorded on a tungsten-25at.% rhenium alloy and a pure tungsten specimen. In the case of the pure tungsten specimen the five naturally occurring isotopes of tungsten (W^{180}, W^{182}, W^{183}, W^{184}, and W^{186}) can be readily distinguished from one another in the W^{+3} spectrum which contains 6009 events. This W^{+3} spectrum was recorded with the atom-probe FIM at a background pressure of 6×10^{-10} torr, at a tip temperature of $\sim$25K and with the probe-hole in the internal image intensification system over the (551) plane. The drift distance of the ions in the flight tube is 1600.3mm. A comparison of our experimental W^{+3} isotopic abundances with the handbook values of these quantities is shown in Table 1. It is seen that the agreement is rather good.

Figure 6. A spectrum of W^{+3} recorded at ~25K in a background pressure of 6×10^{-10} torr is seen in the bottom half of the figure. The top half of the figure shows the W^{+3} and Re^{+3} spectrum for a W-25at.% Re alloy. Note the clear separation of the rhenium isotopes from the tungsten isotopes.

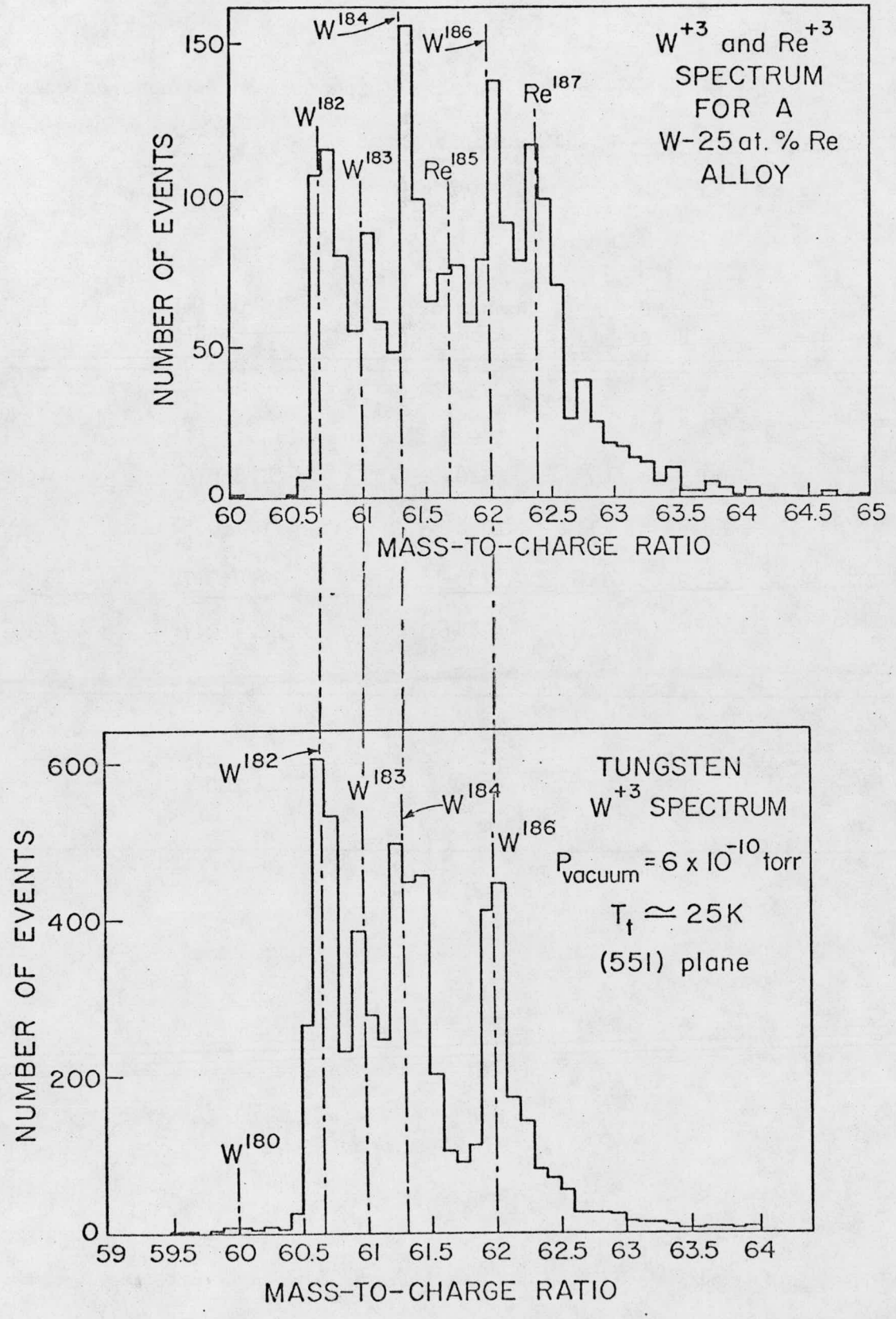
W184
W186
W182
W183
Re185
Re187
W+3 and Re+3
SPECTRUM
FOR A
W-25 at. % Re
ALLOY
NUMBER OF EVENTS
MASS-TO-CHARGE RATIO
TUNGSTEN
W+3 SPECTRUM
Pvacuum = 6 x 10-10 torr
Tf ≃ 25K
(551) plane
W180

Figure 6

Table 1: Comparison of our experimental W^{+3} isotopic abundances calculated from Fig. 6 and the actual isotopic abundances.

Isotope	AMU Range	Number of Atoms	Experimental %	Actual %
W^{180}	59.8 to 60.2	20±4	0.33±0.07	0.14
W^{182}	60.5 to 60.85	1520.5±39	25.3±0.6	26.41
W^{183}	60.85 to 61.2	1026.5±32	17.1±0.5	14.4
W^{184}	61.2 to 61.8	1789±42	29.9±0.7	30.64
W^{186}	61.8 to 64.0	1644±41	27.4±0.7	28.41
Totals		6009	100	100

The W^{+3} and Re^{+3} spectrum shown in the top of figure 6 is for a tungsten-25at.% rhenium specimen. The spectrum was recorded at a tip temperature of 25K employing a drift distance of 2232mm. The $^{185}Re^{+3}$ peak at 61.67amu and the $^{187}Re^{+3}$ peak at 62.33amu are readily seen. A comparison of our experimental isotopic abundances with the handbook values is given for the W-25% Re alloy in Table 2. The total Re concentration is 28.5at.%. This result was obtained counting only those atoms in the ranges shown in Table 4. In contrast, the 25.4at.% Re result obtained from the composition profile is the number of atoms in the ranges 61.6 to 62.0 and 62.3 to 62.6 divided by the total number of atoms in the $W\text{-}Re^{+3}$ peak including the tail from 62.6 to 65amu.

Clearly there is a problem in accounting for the atoms in the tail in a simple way because each peak has its own tail which interferes with the peaks at higher (m/n). To resolve this a third method was used to obtain the relative concentration of rhenium. A relatively simple least-squares procedure was used to fit all seven peaks in the $W\text{-}Re^{+3}$ spectrum assuming they are of pure exponential form. The adjustable parameters were the concentration of rhenium and the decay constant of the exponential tail. In addition a third parameter, which compensated for any error in the absolute position of the m/n spectrum, was least-squares adjusted. The results of the fit were 22±2% for the rhenium concentration, 0.31amu for the decay constant of the exponential tail, and 0.065amu for the required shift in the m/n scale to obtain the best fit.

(b) Molybdenum and Molybdenum Alloys

In preparation for a study on a series of neutron irradiated molybdenum alloys a number of preliminary experiments on molybdenum and molybdenum alloys were performed. Because the amount of irradiated material is very limited, extensive specimen development was performed on commercial samples of molybdenum and a titanium-zirconium-molybdenum (TZM) alloy. After developing a successful FIM specimen preparation technique for molybdenum and TZM, runs were made on these materials to test that the atom-probe FIM experiments were possible. As indicated in sections i and ii below

Table 2: A comparison of the experimental W-25% Re^{+3} isotopic abundances with actual isotopic abundances.

(a) Tungsten Isotopes

Isotope	AMU Range	Number of Atoms	Experimental %	Actual %
W^{180}	59.9 to 60.4	1	0.1±0.1	0.1
W^{182}	60.4 to 60.9	310	24.7±1.4	26.4
W^{183}	60.9 to 61.3	243	19.3±1.2	14.4
W^{184}	61.3 to 61.6	394	31.4±1.6	30.7
W^{186}	62.0 to 62.3	307	24.5±1.4	28.4
Totals		1255	100.0	100.0

(b) Rhenium Isotopes

Isotope	AMU Range	Number of Atoms	Experimental %	Actual %
Re^{185}	61.6 to 62.0	214	42.8±3.1	37.1
Re^{187}	62.3 to 62.6	286	57.2±3.1	62.9
Totals		500	100.0	100.0

(c) Relative Concentrations

Element	Number of Atoms	Experimental %	Nominal* %
W	1255	71.5±1.6	75.0
Re	500	28.5±1.6	25.0
Totals	1755	100.0	100.0

* Based on nominal concentrations for W-25at.% Re.

these experiments were successful. The titanium and zirconium were clearly distinguishable from one another and the measured concentrations agreed with the nominal concentrations.

The same techniques were also successfully applied to the as-received, irradiated samples which serve as controls for the neutron-irradiated specimens. The experiments on the neutron irradiated specimens are presently in progress.

(i) Molybdenum

A histogram of the Mo^{+2} spectrum is shown in Figure 7. The peaks associated with the seven naturally occurring isotopes of Mo (Mo^{92}, Mo^{94}, Mo^{95}, Mo^{96}, Mo^{97}, Mo^{98}, Mo^{100}) are clearly distinguishable from one another. The Mo^{+2} spectrum was recorded with the atom-probe FIM at a background pressure of 5×10^{-9} torr, at a tip temperature of ≃60K, and with the probe hole in the image intensification system near the (110) pole; the drift distance was 2213mm. A comparison of our experimental Mo^{+2} isotopic abundances with the handbook values of these quantities is shown in Table 3. It is seen that there is good agreement between the two sets of values.

(ii) Titanium-Zirconium-Molybdenum (TZM)

Figure 8 shows a portion of the Mo^{+3} and Zr^{+3} spectrum. The $^{90}Zr^{+3}$ peak is readily distinguished from the Mo^{+3} peaks. The Zr^{+3} isotopes ^{92}Zr, ^{94}Zr and ^{96}Zr clearly cannot be distinguished from the Mo^{+3} isotopes ^{92}Mo, ^{94}Mo and ^{96}Mo. No evidence was found for the Zr^{91} isotope in the +3 charge state. This isotope should have appeared at 30.33amu. It did not appear, most likely, because its isotopic abundance is only 11.23% compared with an isotopic abundance of 51.46% for the ^{90}Zr isotope; thus we could expect only ∿1 event for this isotope in the +3 charge state for the total number of Mo^{+3} ions counted (≳10,000).

Analysis of the spatial distribution of the titanium and zirconium showed that the titanium was randomly distributed while all the zirconium was contained in a single cluster. This single cluster of zirconium was detected just before the

Figure 7. The Mo^{+2} spectrum for a specimen pulse-field evaporated at a specimen temperature between 57 and 69K with the dc voltage varying continuously from 11.6 to 15.5kV.

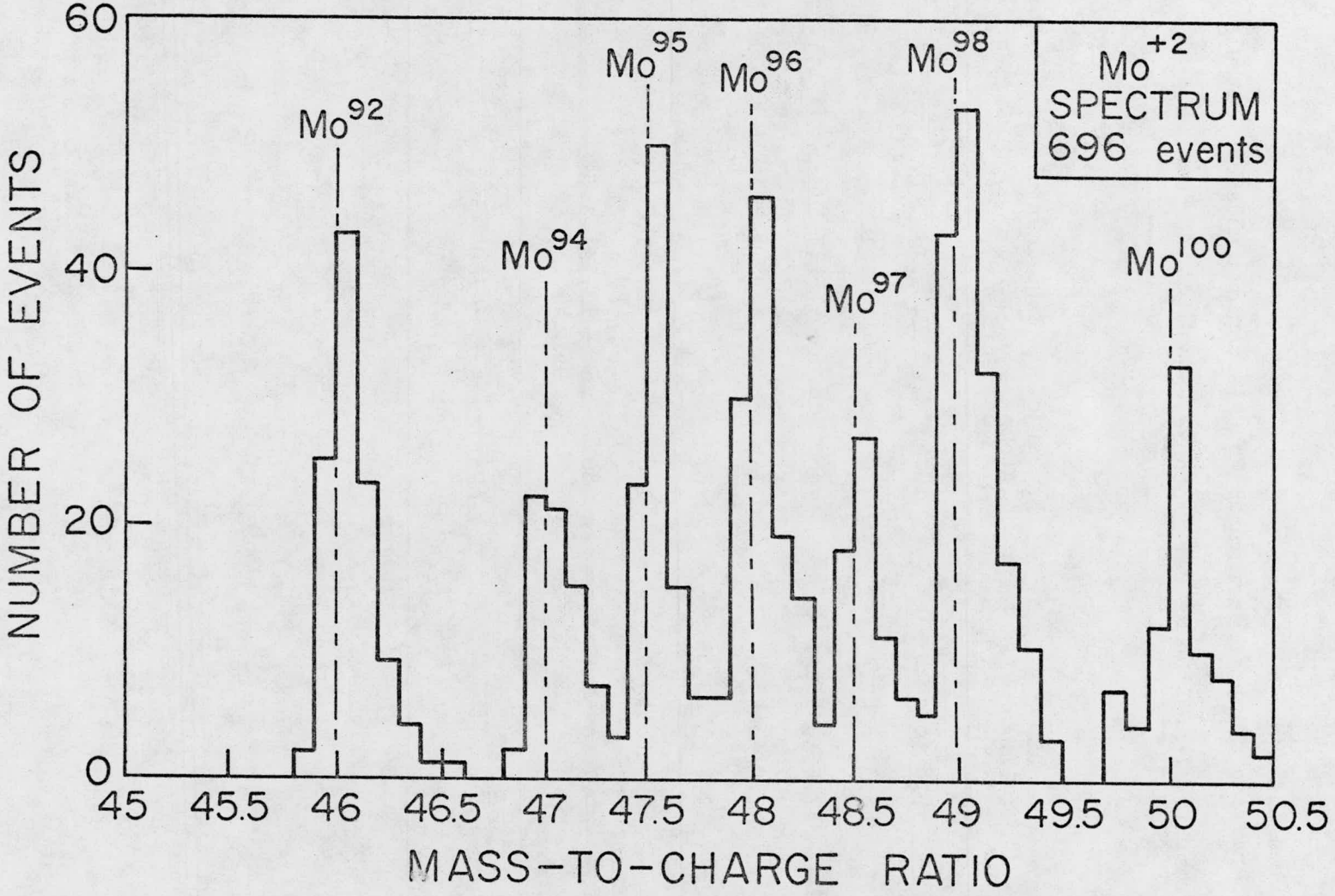
60
40
20
0
NUMBER OF EVENTS
Mo92
Mo94
Mo95
Mo96
Mo97
Mo98
Mo100
Mo+2
SPECTRUM
696 events
45
45.5
46
46.5
47
47.5
48
48.5
49
49.5
50
50.5
MASS-TO-CHARGE RATIO

Figure 7

Table 3: Comparison of the experimental Mo^{+2} isotopic abundances calculated from Fig. 7 and the actual isotopic abundances.

Isotope	AMU Range	Number of Atoms	Experimental %	Actual %
Mo^{92}	45.8 to 46.6	108	15.5±1.5	15.84
Mo^{94}	46.8 to 47.4	70	10.1±1.2	9.04
Mo^{95}	47.4 to 47.9	100	14.4±1.4	15.72
Mo^{96}	47.9 to 48.4	113	16.2+1.5	16.53
Mo^{97}	48.4 to 48.9	67	9.6±1.2	9.46
Mo^{98}	48.9 to 49.5	158	22.6±1.8	23.78
Mo^{100}	49.7 to 50.5	80	11.5±1.3	9.63
Totals		696	100	100

Figure 8. The Mo^{+3} and Zr^{+3} spectrum for a TZM alloy. The spectrum was recorded with the vacuum in the atom-probe FIM at a background pressure of 4.8×10^{-10} torr and with the specimen at a temperature of 41K.

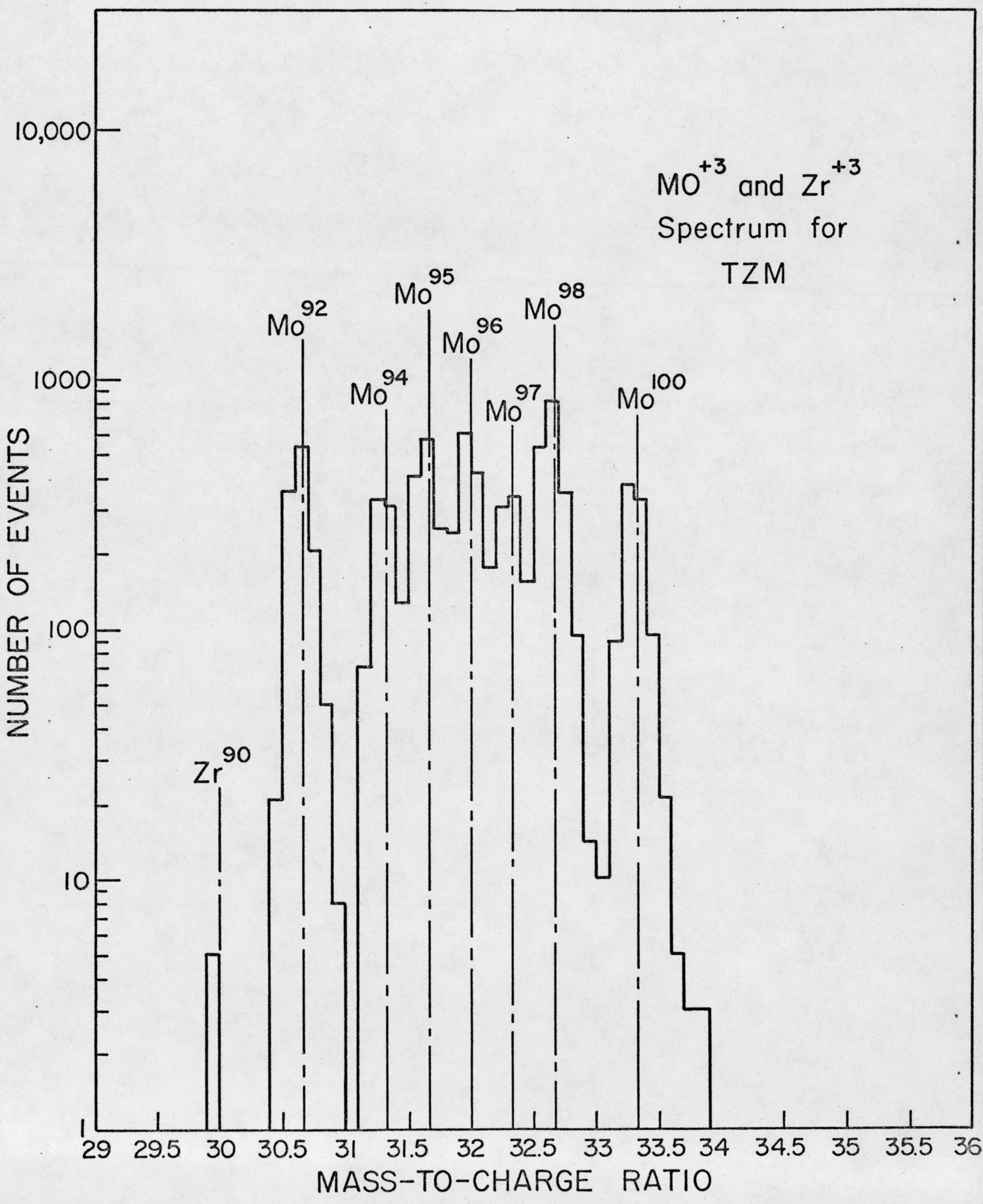
MO+3 and Zr+3
Spectrum for
TZM
Zr90
Mo92
Mo94
Mo95
Mo96
Mo97
Mo98
Mo100
NUMBER OF EVENTS
10,000
1000
100
10
1
29
29.5
30
30.5
31
31.5
32
32.5
33
33.5
34
34.5
35
35.5
36
MASS-TO-CHARGE RATIO

Figure 8

tip failed, and could have contributed to the failure of the tip. These experiments on TZM indicated that both the titanium and zirconium alloying elements in the $\lesssim$lat.% concentration range could be detected and that the techniques developed should work reasonably well for irradiated specimens.

(iii) Molybdenum-(titanium)

Atom-probe FIM experiments were performed on unirradiated specimens of the Mo-0.5wt.% Ti alloy. These specimens will serve as a control for a series of neutron irradiated Mo-0.5wt.% Ti alloys. Both sets of specimens were kindly supplied by Prof. John Moteff of the University of Cincinnati. The Mo-0.5wt.% Ti alloys exhibited on enhanced swelling behavior when compared to the molybdenum specimens irradiated under identical conditions to the same fast neutron dose. It is the purpose of the present experiment to determine the role played by the titanium in the swelling behavior of neutron irradiated molybdenum. It is interesting to note that Johnston et al. (31) have found Ti to be a particularly effective swelling inhibitor in a series of model Fe-Ci-Ni alloys.

The Ti^{+3} spectrum for the as-received Mo-0.5wt.% Ti alloly is shown in Figure 9. The five isotopes of Ti (Ti^{46}, Ti^{47}, Ti^{48}, Ti^{49} and Ti^{50}) are very clearly seen in this figure. Table 4 shows a comparison of the experimental Ti^{+3} isotopic abundances with the actual isotopic abundances. The agreement is reasonable considering that the sample size only involved 30 Ti^{+3} ions for all five isotopes. The Ti was also found to be randomly distributed throughout the alloy. This is significant because a comparison of the present results with the results on the irradiated Mo-(Ti) alloys should allow us to comment in detail on the changes produced in the spatial distribution of Ti atoms in the alloy as a result of the fast neutron irradiation.

(c) A low swelling stainless steel alloy (LSIA)

A low swelling stainless steel alloy (LSIA) developed at the Oak Ridge National Laboratory (ORNL), and kindly supplied to us by Dr. L. K. Mansur, has been analyzed by the atom-probe FIM technique. To date we have restricted our work to unirradiated

Figure 9. A Ti^{+3} spectrum for a Mo-0.5wt.% Ti alloy.

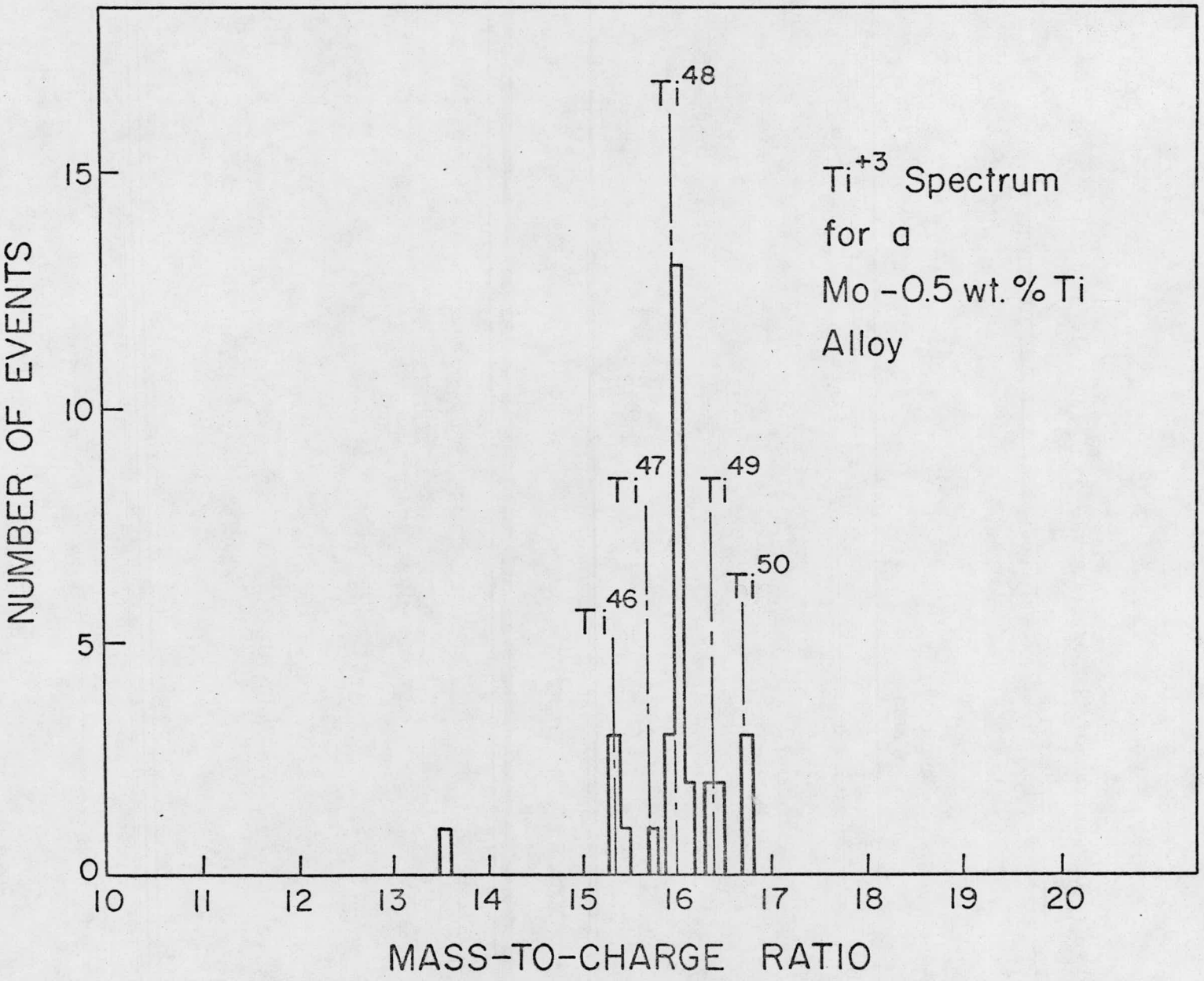
NUMBER OF EVENTS
15
10
5
0
10
11
12
13
14
15
16
17
18
19
20
MASS-TO-CHARGE RATIO
Ti48
Ti47
Ti49
Ti46
Ti50
Ti+3 Spectrum
for a
Mo -0.5 wt. % Ti
Alloy

Figure 9

Table 4: Comparison of the experimental Ti^{+3} isotopic abundance in an as-received Mo-0.5wt.% Ti alloy and the actual isotopic abundances.

Isotope	Number of Atoms	Experimental %	Actual %
Ti^{46}	4	13±7	7.9
Ti^{47}	1	3±3	7.3
Ti^{48}	18	60±14	73.9
Ti^{49}	4	13±7	5.5
Ti^{50}	3	10±6	5.4
TOTALS	30	99	100

specimens of this alloy because of the high radioactivity of the neutron irradiated specimens. The alloy LSIA contains 2.06at.% Si and 0.16at.% as swelling inhibitors. Table 5 shows the composition of each element in this alloy as determined by the atom-probe FIM technique. The last column in the table gives the chemical composition as supplied to us by ORNL. It is seen that the basic agreement between the two techniques, is good. All the alloying elements (Fe, Cr, Ni, Mn, Mo, C, Si, and Ti) in LSIA were readily identified by the atom-probe FIM technique. Figure 10 shows the isotopes $^{52}Cr^{+4}$, $^{28}Si^{+2}$, $^{29}Si^{+2}$, $^{30}Si^{+2}$ and $^{48}Ti^{+3}$ in the 12 to 17amu part of the spectrum. The $^{48}Ti^{+2}$ peak could contain an undetermined amount of oxygen. The most probable source of the oxygen is residual carbon dioxide in the FIM which can decompose on the surface of the FIM tip. Figure 11 shows the isotopes $^{50}Cr^{+2}$, $^{52}Cr^{+2}$, $^{54}Fe^{+2}$, $^{55}Mn^{+2}$, $^{56}Fe^{+2}$, $^{58}Ni^{+2}$ and $^{60}Ni^{+2}$ in the 24 to 34amu portion of the spectrum. The spectra for the LSIA alloy were recorded with the atom-probe FIM at a background pressure of $1x10^{-9}$torr and at a tip temperature of ~50K.

An analysis of the spatial distribution of the various alloying elements showed the existence of one large cluster consisting of three silicon atoms, two carbon atoms and two titanium (or possibly oxygen) atoms. It is highly improbable for such a cluster to form randomly for these rather low concentration alloying elements. This result indicates the existence of a positive binding enthalpy between carbon and silicon (and possibly titanium) in this LSIA alloy.

H. The Range of a Focused Collision Replacement Sequence in Ordered Alloys

In a recent study of partially ordered Ni_3Mn irradiated with thermal neutrons Kirk et al. (32) claim to have developed a technique to measure the averave length of a focused collision replacement sequence. These workers have measured the change in magnetic saturation with dose for different values of the long-range order-parameter(S). The change in magnetic saturation with dose was measured for S equal to approximately 0.79, 0,90 and 0.95. A quantitative computer analysis of the magnetic disorder produced by <111> focused collision replacement sequences

Table 5: Comparison of the composition of a low swelling stainless steel (LS1A) as determined by the Atom Probe and by chemical analysis

Element	Atom Probe Analysis Atomic %	Chemical Analysis Atomic %
Fe	62.2 ± 1.1	63.96
Cr	14.5 ± 0.5	17.4
Ni	16.2 ± 0.6	12.9
Mn	2.6 ± 0.2	2.0
Mo	1.8 ± 0.2	1.0
C	0.4 ± 0.1	0.37
Si	1.7 ± 0.2	2.06
Ti	0.2 ± 0.06	0.16
Other	.5 ± 0.1	0.15

Figure 10. The Cr^{+4}, Si^{+2} and Ti^{+3} spectrum for a LSIA alloy in the 12 to 17amu portion of the spectrum.

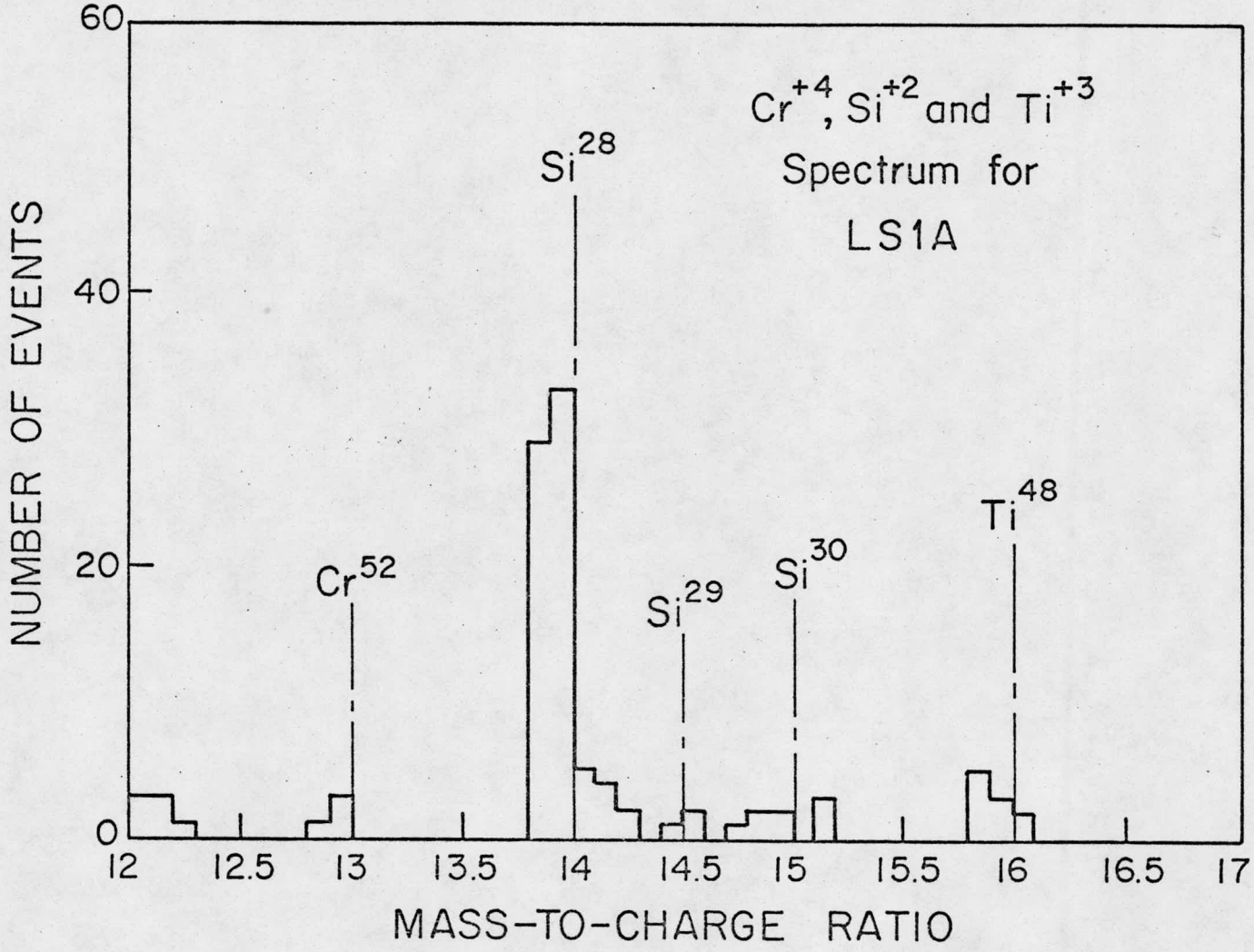
60
40
20
0
NUMBER OF EVENTS
12
12.5
13
13.5
14
14.5
15
15.5
16
16.5
17
MASS-TO-CHARGE RATIO
Cr+4, Si+2 and Ti+3
Spectrum for
LS1A
Si28
Cr52
Si29
Si30
Ti48

Figure 10

Figure 11. The Fe^{+2}, Cr^{+2}, Ni^{+2} and Mn^{+2} and Mn^{+2} spectrum for LSIA in the 24 to 34amu portion of the spectrum.

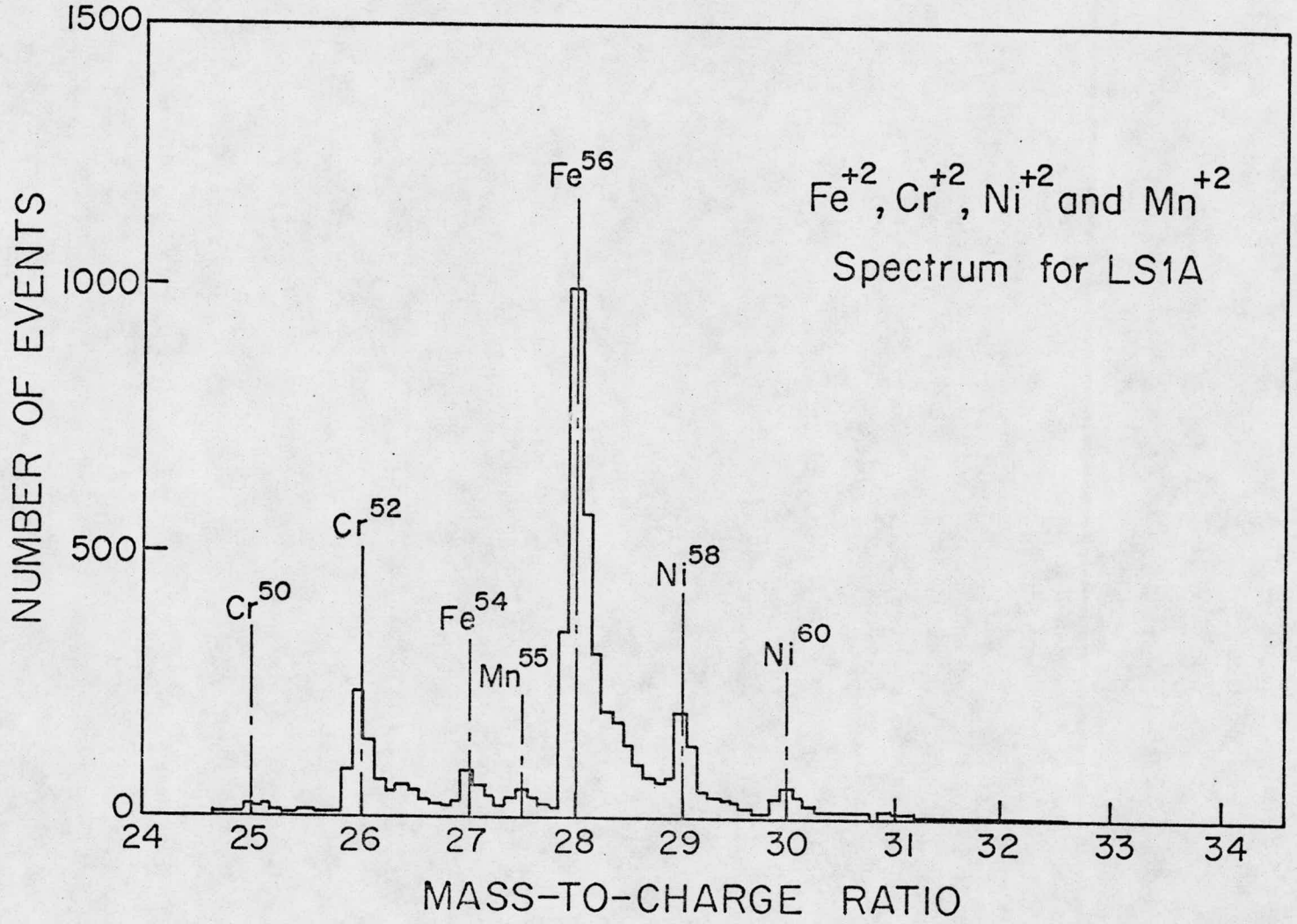
1500
1000
500
0
NUMBER OF EVENTS
Fe+2, Cr+2, Ni+2 and Mn+2
Spectrum for LS1A
Cr50
Cr52
Fe54
Mn55
Fe56
Ni58
Ni60
24
25
26
27
28
29
30
31
32
33
34
MASS-TO-CHARGE RATIO

Figure 11

showed that the magnetic disorder caused by a focused collision replacement sequence is a maximum at S=0.7 and decreases to zero at S=1. Kirk et al. calculated from their data an average sequence length of about 50 atoms along the <110> direction.

We are presently studying the random disordering produced by focused collision replacement sequences in Ni_4Mo by direct observation in the FIM. The ideas pertinent to the experiment are as follows. If one starts with a fully ordered alloy (S=1) then the FIM image of this alloy resembles that of a pure metal (33,34). The result of the lattice disorder produced by the focused replacement sequences is to change the image contrast to that which is characteristic of a random alloy (34). A specimen of the fully ordered alloys is irradiated in-situ with low energy neon ions (<1000eV) so that all the vacancies are left at the irradiated surface and the interstitials are driven into the bulk of the FIM specimen by the focused collision replacement sequence mechanism. After the irradiation the specimen is pulse field evaporated and the measured width of the disordered region (as detected by its random appearance) is used as a measure of the range of the focused collision replacement sequence.

During the past year much of the experimental effort had been expended on the preparation of ordered alloys of both Ni_3Mn and Ni_4Mo. The alloy Ni_3Mn proved to be particularly difficult alloy to order because of the low temperature (425°C) at which the order parameter is equal to unity. Hence, we switched to the alloy Ni_4Mo for the following two reasons: (1) It achieves a long-range order-parameter of unity with a large domain size in relatively short times (a few hours); and (2) it is possible to obtain high quality FIM images of this structure fairly readily (35). Thus, the main progress in this area has been the production of ordered alloys of Ni_4Mo and the imaging of these specimens. Several preliminary irradiation experiments have been performed and the initial indications are quite exciting. It is noted that this tehcnique is applicable to a large number of ordered alloys which are imagable by the FIM technique (e.g., Ni_3Fe and Ni_3Al). It is therefore proposed

to extend our experiments to other systems to look at the effect of the difference in atomic mass between the two alloying elements on the length of the focused replacement sequence chain.

I. The Interaction of Self-Interstitial Atoms With Impurity Gas Solute Atoms in Refractory Metals.

This problem involves the preparation of alloys of refractory metals and the in-situ irradiation of the specimens with low energy (~1000eV) xenon ions. At less than 1000eV the main mechanism for self-interstitial production will be via the focused replacement collision sequence mechanism. The alloy specimens are irradiated in-situ at a temperature which is above substage I_E so that the SIA's produced are mobile. The SIA's then migrate towards both the sinks and the solute atoms and in the process clusters of complexes are formed. We are trying to study both the SIA solute atom clusters and also any self-clusters that form. Towards this end we have constructed a quenching system to dope specimens with various gas atoms. Our initial efforts have centered on the Group VB metal tantalum, as this metal has a high solubility for a number of gases (e.g., O_2, H_2, and N_2) and is also readily imaged by the FIM technique (36,37). During the past year the quenching system has been operational for introducing gases into metal systems. In addition, we have started to prepare FIM specimens of Ta. It is expected that Ta-(O) specimens will, in the near future, be irradiated in-situ in the atom-probe FIM.

III. Other Financial Assistance

A total of $23,735 was received from the National Science Foundation through the Cornell Materials Science Center at Cornell University. Included in this sum was one month of summer salary plus overhead funds for Professor D. N. Seidman. It is proposed to reduce Professor Seidman's support from the Materials Science Center to two weeks for the contract period May 1, 1976 to April 30, 1977. The research performed with this Materials Science Center support consisted of some

initial feasability studies for the "Construction of a Field-Desorption Microscope" and a study of "Clustering Effects in Metallic Glasses". The metallic glasses were composed of iron, nickel, boron and phosphorous.

IV. List of Documents Generated During the Contract Period

1. "A Simplified Method for the Calibration of an Atom-Probe Field-Ion Microscope", A. Wagner, T.M. Hall, D.N. Seidman, COO-3158-40.
2. "An In-Situ Field-Ion Microscope Study of Irradiated Tungsten and Tungsten Alloys: II. The Recovery Behavior in Stages I and II - Analysis and Discussion", K.L. Wilson and D. N. Seidman, COO-3158-41.
3. "The Search for the Stage III Self-Interstitial Atom in Electron-Irradiated Tungsten", K.L. Wilson and D.N. Seidman, COO-3158-42.
4. "An In-Situ Field-Ion Microscope Study of the Recovery Behavior of Stage II in a Series of Ion-Irradiated Platinum - 0.10, 0.62 and 4.0at.% Gold Alloys", COO-3158-43.
5. "Long-Range Migration of Self-Interstitial Atoms in Tungsten", D.N. Seidman, K.L. Wilson and C.H. Nielsen, COO-3158-44.
6. "The Study of Stages I to IV of Irradiated or Quenched Tungsten and Tungsten Alloys by Field-Ion Microscopy", D.N. Seidman, K.L. Wilson and C.H. Nielsen, COO-3158-45.
7. "Field-Ion Microscope Studies of the Defect Structure of the Primary State of Damage of Irradiated Metals", D. N. Seidman, COO-3158-46.
8. "A Time-of-Flight Atom-Probe Field-Ion Microscope for the Study of Defects in Metals", T.M. Hall, A. Wagner, A.S. Berger and D.N. Seidman, COO-3158-47.
9. Annual Progress Report, "Defects in Metal Crystals", D.N. Seidman, COO-3158-48.

REFERENCES

1. R.M. Scanlan, D.L. Styris and D.N. Seidman, Phil. Mag. 23, 1439 (1971).
2. R.M. Scanlan, D.L. Styris and D.N. Seidman, Phil. Mag. 23, 1459 (1971).
3. K.L. Wilson and D.N. Seidman, Cornell Materials Science Center Report #2346 (1974). Accepted for publication in Radiation Effects (1975).
4. K.L. Wilson and D.N. Seidman, Cornell Materials Science Center Report #2347 (1975).
5. D.N. Seidman, K.L. Wilson and C.H. Nielsen, Phys. Rev. Lett. 35, 1041 (1975).
6. S. Okuda and H. Mizubayashi, Phys. Rev. Lett. 34, 815 (1975).
7. F. Dausinger and H. Schultz, preprint of a paper submitted to Phys. Rev. Lett. (Aug. 1975).
8. C. H. Nielsen, M.S. Thesis, Cornell University (1976).
9. C-Y. Wei and D.N. Seidman, Cornell Materials Science Center Report No. 2398 (1975).
10. C-Y. Wei, M.S. Thesis, Cornell University (1975).
11. K.L. Wilson and D.N. Seidman, Cornell Materials Science Center Report No. 2518 (1975).
12. D.N. Seidman, K.L. Wilson and C.H. Nielsen, Cornell Materials Science Center Report No. 2524 (1975).
13. M.J. Attardo, J.M. Galligan and J.G.Y. Chow, Phys. Rev. Lett. 19, 73 (1967).
14. W. Kunz and H. Schultz, in Proc. of the Inter. Meeting on Defects in Refractory Metals, edtied by R. de Batist, J. Nihoul and L. Staals, p. 99, Studiecentrum voor kern energie, Mol, Belgium, 1972.
15. R.J. Gripshover, M. Koshnevisan, J.S. Zetts and J. Bass, Phil. Mag. 22, 757 (1970).
16. W. Kunz, K. Faber, R. Lachenmann and H. Schultz, p. 7 in Ref. 14.

17. J.Y. Park, H-C. W. Huang, A.S. Berger and R.W. Balluffi, in Nuclear Energy, Proc. 1973. Inter. Conf. on Defects and Defect Clusters in B.C.C. Metals and Their Alloys, edited by R. Arsenault, p. 420, Vol. 18, National Bureau of Standards, Gaithersburg, Maryland, 1973.

18. D.N. Seidman, Cornell Materials Science Center Report No. 2564 (1975).

19. L.A. Beavan, R.M. Scanlan and D.N. Seidman, Acta Met. 19, 1339 (1971).

20. K.L. Wilson and D.N. Seidman, p. 216 in Ref. 17.

21. C.A. English, B.L. Eyre and J. Summers, Harwell Report AERE-R7960 (1975).

22. M. Wilkens in Vacancies and Interstitials in Metals, edited by A. Seeger, D. Schumacher, W. Schilling and J. Diehl (Worth-Holland, Amsterdam, 1970) p. 485.

23. B. L. Eyre, p. 311 in Ref. 14.

24. M. Wilkens, to appear in the proceedings of Fundamental Aspects of Radiation Damage in Metals, (Gatlinburg, Tennessee, Oct. 1975).

25. R. H. Silsbee, J. Appl. Phys. 28, 1246 (1957).

26. K. H. Ecker, Rad. Effects 23, 171 (1974).

27. F. Dworschak, H.-E. Schepp and H. Wollenberger, J. Appl. Phys. 46, 1049 (1975).

28. D.N. Seidman, U.S. Atomic Energy Commission Report No. COO-3158-39 (1975).

29. T.M. Hall, A. Wagner, A.S. Berger and D.N. Seidman, Cornell Materials Science Center Report No. 2357 (1975).

30. A. Wagner, T.M. Hall and D.N. Seidman, Rev. Sci. Instrum. 46, 1032 (1975).

31. W. G. Johnston, T. Lauritzen, J.H. Rosolowski and A.M. Turkalo, General Electric, Schenectady, New York, Report No. 76CRD019 (1976).

32. M.A. Kirk, T.H. Blewitt, A.C. Klank and T.L. Scott, Argonne National Laboratory, Report, Materials Science Division (1974).

33. R.J. Taunt, R. Sinclair, and B. Ralph, Phys. Stat. Sol. (a) 16, 469 (1973).

34. B.G. LeFevre, Surface Sci. 23, 114 (1970).

35. P.R. Okamoto and G. Thomas, Acta Met. (1971).

36. S. Nakamura and E.W. Müller, J. Appl. Phys. 36, 2535 (1965).

37. S. Nakamura and E.W. Müller, J. Appl. Phys. 36, 3634 (1965).